

RtEstim: Effective reproduction number estimation with trend filtering

Jiaping Liu^{1*}, Zhenglun Cai², Paul Gustafson¹, Daniel J. McDonald¹

1 Department of Statistics, The University of British Columbia, Vancouver, British Columbia, Canada

2 Centre for Health Evaluation and Outcome Sciences, The University of British Columbia, Vancouver, British Columbia, Canada

* jiaping.liu@stat.ubc.ca

Abstract

To understand the transmissibility and spread of infectious diseases, epidemiologists turn to estimates of the effective reproduction number. While many approaches exist, their utility may be limited by the challenges of surveillance data collection. Arbitrary model assumptions that are unverifiable with data alone and sophisticated, though computationally inefficient, frameworks are critical limitations for many existing approaches. We propose a discrete spline-based approach **RtEstim** that solves a convex optimization problem — Poisson trend filtering — using the proximal Newton method. It produces a locally adaptive estimator for effective reproduction number estimation with heterogeneous smoothness. **RtEstim** remains accurate even under some process misspecifications and is computationally efficient, even for large-scale data. The implementation is easily accessible in a lightweight R package **rtestim**.

Keywords: discrete splines | piecewise polynomials

Author summary

Effective reproduction number estimation presents many challenges, for example, data is usually collected from multiple sources and there are reporting delays. This cause many

problems, such as missing values, underreporting and lack of standardization. Such data limitations hinder the accurate estimation of effective reproduction number. Our motivation is to develop a model that returns accurate estimation, is robust to model misspecification, and is straightforward to use and computationally efficient, even for large-scale data. We propose a convex optimization model with an ℓ_1 trend filtering penalty for univariate data. It involves temporal evolution of the effective reproduction number for a user-selected level of curvature. We solve our model using the proximal Newton method, which converges rapidly and is numerically stable. Our software, R package **RtEstim**, can return the output in seconds for univariate incidence sequences with hundreds of observations across a series of tuning parameters using cross validation.

1 Introduction

The effective reproduction number (also called the instantaneous reproduction number) is a key quantity for understanding infectious disease dynamics including the potential size of a pandemic, the required stringency of prevention measures, and the efficacy of other controls. The effective reproduction number is defined to be the average number of secondary infections caused by a new primary infection that occurs at a specific time. Tracking the time series of this quantity is therefore useful for understanding whether or not future infections are likely to increase or decrease from the current state. Let $\mathcal{R}(t)$ denote the effective reproduction number at time t . Practically, as long as $\mathcal{R}(t) < 1$, infections will decline gradually, eventually resulting in a disease-free equilibrium, whereas when $\mathcal{R}(t) > 1$, infections will continue to increase, resulting in endemic equilibrium. While $\mathcal{R}(t)$ is fundamentally a continuous time quantity, it can be related to data only at discrete points in time $t = 1, \dots, n$. This sequence of effective reproduction numbers over time is not observable, but, nonetheless, is easily interpretable and retrospectively describes the course of an epidemic. Therefore, a number of procedures exist to estimate \mathcal{R}_t from different types of observed incidence data such as cases, deaths, or hospitalizations, while relying on various domain-specific assumptions. Importantly, accurate estimation of effective reproduction numbers relies heavily on the quality of the available data, and, due to the limitations of data collection, such as underreporting and lack of standardization, estimation methodologies

rely on various assumptions to compensate. Because model assumptions may not be easily verifiable from data alone, it is also critical for any estimation procedure to be robust to model misspecification.

Many existing approaches for effective reproduction number estimation are Bayesian: they estimate the posterior distribution of \mathcal{R}_t conditional on the observations. One of the first such approaches is the software **EpiEstim** [1], described by [2]. This method is prospective, in that it uses only observations available up to time t in order to estimate \mathcal{R}_t for each $i = 1, \dots, t$. An advantage of **EpiEstim** is its straightforward statistical model: new incidence data follows the Poisson distribution conditional on past incidence combined with the conjugate gamma prior distribution for \mathcal{R}_t with fixed hyperparameters. Additionally, the serial interval distribution, the distribution of the period between onsets of primary and secondary infections in a population, is fixed and known. For this reason, **EpiEstim** requires little domain expertise for use, and it is computationally fast. [3] modified this method to distinguish imported cases from local transmission and simultaneously estimate the serial interval distribution. [4] further extended **EpiEstim** by using “reconstructed” daily incidence data to handle irregularly spaced observations. [5] proposed a Bayesian latent variable framework, **EpiNow2** [6], which leverages incident cases, deaths or other available streams simultaneously along with allowing additional delay distributions (incubation period and onset to reporting delays) in modelling. [7] proposed an extension that handles missing data by imputation followed by a truncation adjustment. These modifications are intended to increase accuracy at the most recent (but most uncertain) timepoints, to aid policymakers. [8] also proposed a Bayesian approach, **EpiFilter** based on the (discretized) Kalman filter and smoother. **EpiFilter** also estimates the posterior of \mathcal{R}_t given a Gamma prior and Poisson distributed incident cases. Compared to **EpiEstim**, however, **EpiFilter** estimates \mathcal{R}_t retrospectively using all available incidence data both before and after time t , with the goal of being more robust in low-incidence periods. [9] proposed a Bayesian P-splines approach, **EpiLPS**, that assumes negative Binomial distributed incidence. [10] also proposed a Bayesian model estimated with particle filtering to incorporate spatial structures. Bayesian approaches estimate the posterior distribution of the effective reproduction numbers and possess the advantage that credible intervals may be easily computed. A limitation of many Bayesian approaches, however, is that they usually

require more intensive computational routines, especially when observed data sequences are long or hierarchical structures are complex. Below, we compare our method to two of the more computationally efficient Bayesian models, **EpiEstim** and **EpiLPS**.

There are also frequentist approaches for \mathcal{R}_t estimation. [11] proposed regularizing the smoothness of \mathcal{R}_t through penalized regression with second-order temporal regularization, additional spatial penalties, and with Poisson loss. [12] extended this procedure by introducing another penalty on outliers. [13] proposed a spline-based model relying on the assumption of exponential-family distributed incidence. [14] estimates \mathcal{R}_t while monitoring the time-varying level of overdispersion. There are other spline-based approaches such as [15, 16], autoregressive models with random effects [17] that are robust to low incidence, and generalized autoregressive moving average (GARMA) models [18] that are robust to measurement errors in incidence data.

We propose a retrospective effective reproduction number estimator called **RtEstim** that requires only incidence data. Our model makes the conditional Poisson assumption, similar to much of the prior work described above, but is empirically more robust to misspecification. This estimator is defined by a convex optimization problem with Poisson loss and ℓ_1 penalty on the temporal evolution of $\log(\mathcal{R}_t)$ to impose smoothness over time. As a result, **RtEstim** generates discrete splines, and the estimated curves (in logarithmic space) appear to be piecewise polynomials of an order selected by the user. Importantly, the estimates are locally adaptive, meaning that different time ranges may possess heterogeneous smoothness. Because we penalize the logarithm of \mathcal{R}_t , we naturally accommodate the positivity requirement, can handle large or small incidence measurements, and are automatically (reasonably) robust to outliers without additional constraints. A small illustration using three years of Covid-19 case data in Canada is shown in Fig 1.

While our approach is straightforward and requires little domain knowledge for implementation, we also implement a number of refinements. We use a proximal Newton method to solve the convex optimization problem along with warm starts to produce estimates efficiently, typically in a matter of seconds, even for long sequences of data. In a number of simulation experiments, we show empirically that our approach is more accurate than existing methods at estimating the true effective reproduction numbers.

The manuscript proceeds as follows. We first introduce the methodology of **RtEstim**

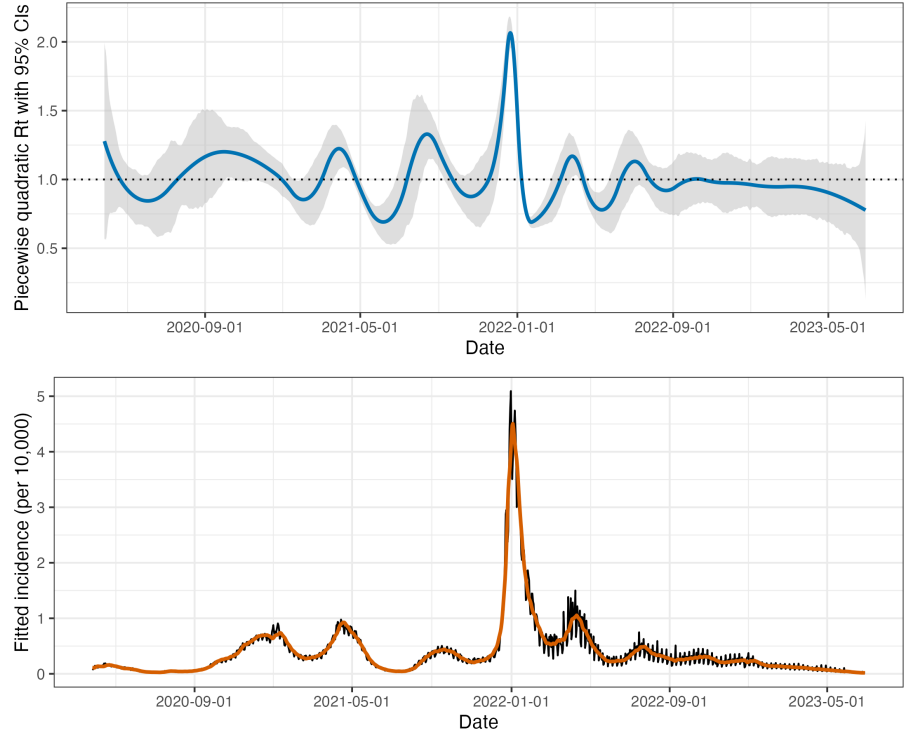


Fig 1. A demonstration of effective reproduction number estimation by `RtEstim` and the corresponding fitted incident cases for the Covid-19 epidemic in Canada during a period from March 28, 2020 to June 28, 2023. The blue curve in the top panel is the estimated piecewise quadratic \mathcal{R}_t and the gray ribbon is the corresponding 95% confidence band. The black curve in the bottom panel is the observed Covid-19 daily confirmed cases, and the orange curve is the fitted incidence corresponding to the estimated \mathcal{R}_t .

including the usage of renewal equation and the development of Poisson trend filtering
estimator. We explain how this method could be interpreted from the Bayesian
perspective, connecting it to previous work in this context. We provide illustrative
experiments comparing our estimator to `EpiEstim` and `EpiLPS`. We then apply our
`RtEstim` on the Covid-19 pandemic incidence in British Columbia and the 1918
influenza pandemic incidence in the United States. Finally, we conclude with a
discussion of the advantages and limitations of our approach and describe practical
considerations for effective reproduction number estimation.

2 Methods

2.1 Renewal model for incidence data

The effective reproduction number $\mathcal{R}(t)$ is defined to be the expected number of secondary infections at time t produced by a primary infection sometime in the past. To make this precise, denote the number of new infections at time t as $y(t)$. Then the total primary infectiousness can be written as $\eta(t) := \int_0^\infty p(i)y(t-i)\mathrm{d}i$, where $p(i)$ is the probability that a new secondary infection is the result primary infection which occurred i time units in the past. The reproduction number is then given as the value that equates

$$\mathbb{E}[y(t) \mid y(j), j < t] = \mathcal{R}(t)\eta(t) = \mathcal{R}(t) \int_0^\infty p(i)y(t-i)\mathrm{d}i, \quad (1)$$

otherwise known as the renewal equation. The period between primary and secondary infections is exactly the generation time of the disease, but given real data, observed at discrete times (say, daily) this delay distribution must be discretized into contiguous time intervals, say, $(0, 1], (1, 2], \dots$, which results in the sequence $\{p_i\}_1^\infty$ corresponding to observations y_t and resulting in the discretized version of Eq (1),

$$\mathbb{E}[y_t \mid y_1, \dots, y_{t-1}] = \mathcal{R}_t\eta_t = \mathcal{R}_t \sum_{i=0}^\infty p_i y_{t-i}. \quad (2)$$

Many approaches to estimating \mathcal{R}_t rely on Eq (2) as motivation for their procedures, among them, **EpiEstim** [2] and **EpiFilter** [8].

In most cases, it is safe to assume that infectiousness disappears beyond τ timepoints ($p_i = 0$ for $i > \tau$) so that the truncated integral of the generation interval distribution $\int_0^\tau p_i \mathrm{d}i = 1$. Generation time, however, is usually unobservable and tricky to estimate, so common practice is to approximate it by the serial interval: the period between the symptom onsets of primary and secondary infections. If the infectiousness profile after symptom onset is independent of the incubation period (the period from the time of infection to the time of symptom onset), then this approximation is justifiable: the serial interval distribution and the generation interval distribution share the same mean. However, other properties may not be similarly shared, and, in general,

the generation interval distribution is a convolution of the serial interval distribution
with the distribution of the difference between independent draws from the delay
distribution from infection to symptom onset. See, for example, [19] for a fuller
discussion of the dangers of this approximation. Nonetheless, treating these as
interchangeable is common [2] and doing otherwise is beyond the scope of this work.
Additionally, we assume that the generation interval (and, therefore, the serial interval),
is constant over time t . That is, the probability $p(i)$ depends only on the gap between
primary and secondary infections and not on the time t when the secondary infection
occurs. For our methods, we will assume that the serial interval can be accurately
estimated from auxiliary data (say by contact tracing, or previous epidemics) and we
will take it as fixed, as is common in existing studies, e.g., [2, 11, 12].

The renewal equation in Eq (2) relates observable data streams (incident cases)
occurring at different time points to the reproduction number given the serial interval.
The fact that it depends only on the observed incident counts makes it reasonable to
estimate \mathcal{R}_t . However, data collection idiosyncrasies can obscure this relationship.
Diagnostic testing targets symptomatic individuals, omitting asymptomatic primary
infections which can lead to future secondary infections. Testing practices, availability,
and uptake can vary across space and time [20, 21]. Finally, incident cases as reported to
public health are subject to delays due to laboratory confirmation, test turnaround
times, and eventual submission to public health [22]. For these reasons, reported cases
are lagging indicators of the course of the pandemic. Furthermore, they do not represent
the actual number of new infections that occur on a given day, as indicated by exposure
to the pathogen. The assumptions described above (constant serial interval distribution,
homogenous mixing, similar susceptibility and social behaviours, etc.) are therefore
consequential. That said, Eq (2) also provides some comfort about deviations from
these assumptions. If y_t is scaled by a constant (in time) describing the reporting ratio,
then it will cancel from both sides. Similar arguments mean that even if such a scaling
varies in time, as long as it varies slowly relative to the set of p_i that are larger than 0,
Eq (2) will be a reasonably accurate approximation, so that \mathcal{R}_t can still be estimated
well from reported incidence data. Finally, even a sudden change in reporting ratio, say
from c_1 for $i = 1, \dots, t_1$ to c_2 for $i > t_1$ would only result in large errors for t in the
neighbourhood of t_1 (where the size of this neighbourhood is again determined by the

effective support of $\{p_i\}$). This robustness to certain types of data reporting issues 150
partially justifies using Eq (2) to calculate \mathcal{R}_t . 151

2.2 Poisson trend filtering estimator 152

We use the daily confirmed incident cases y_t on day t to estimate the observed infectious cases under the model that y_t given previous incident cases y_{t-1}, \dots, y_1 and a constant serial interval distribution follows a Poisson distribution with mean Λ_t . That is,

$$y_t \mid y_1, \dots, y_{t-1} \sim \text{Poisson}(\Lambda_t), \text{ where } \Lambda_t = \mathcal{R}_t \sum_{i=0}^{t-1} p_i y_{t-i} = \mathcal{R}_t \eta_t.$$

Given a history of n confirmed incident counts $\mathbf{y} = (y_1, \dots, y_n)^\top$, our goal is to estimate 153
 \mathcal{R}_t . A natural approach is to maximize the likelihood, producing the MLE: 154

$$\begin{aligned} \hat{\mathcal{R}} &= \operatorname{argmax}_{\mathcal{R} \in \mathbb{R}_+^n} \mathbb{P}(\mathcal{R} \mid \mathbf{y}, \mathbf{p}) = \operatorname{argmax}_{\mathcal{R} \in \mathbb{R}_+^n} \prod_{t=1, \dots, n} \frac{e^{-\mathcal{R}_t \eta_t} (\mathcal{R}_t \eta_t)^{y_t}}{y_t!} \\ &= \operatorname{argmin}_{\mathcal{R} \in \mathbb{R}_+^n} \frac{1}{n} \sum_{t=1}^n \mathcal{R}_t \eta_t - y_t \log(\mathcal{R}_t \eta_t). \end{aligned} \quad (3)$$

This optimization problem, however, is easily seen to yield a one-to-one correspondence 155
between the confirmed cases and the effective reproduction, i.e., $\hat{\mathcal{R}}_t = y_t / \eta_t$, so that the 156
estimated sequence $\hat{\mathcal{R}}$ will have no significant graphical smoothness. 157

The MLE is an unbiased estimator of the true parameter \mathcal{R}_t , but unfortunately has 158
high variance: changes in y_t result in proportional changes in $\hat{\mathcal{R}}_t$. To avoid this 159
behaviour, and to match the intuition that $\mathcal{R}_t \approx \mathcal{R}_{t-1}$, we advocate enforcing 160
smoothness of the effective reproduction numbers. This constraint will decrease the 161
variance, and hopefully lead to more accurate estimation of \mathcal{R} , as long as the 162
smoothness assumption is reasonable. Smoothness assumptions are common (see 163
e.g., [8] or [19]), but the *type* of smoothness assumed is critical. [1] imposes smoothness 164
indirectly by estimating \mathcal{R}_t with moving windows of past observations. The Kalman 165
filter procedure of [8] would enforce in ℓ_2 -smoothness $(\int_0^n (\hat{\mathcal{R}}''(t))^2 dt < C$ for some C), 166
although the algorithm results in $\hat{\mathcal{R}}$ taking values over a discrete grid. [12] produces 167
piecewise-linear $\hat{\mathcal{R}}_t$, which turns out to closely relate to a special case of our 168
methodology. Smoother estimated curves will provide high-level information about the 169

entire epidemic, obscuring small local changes in $\mathcal{R}(t)$, but may also remove the ability to detect large sudden changes, such as those resulting from lockdowns or other major containment policies.

We choose to implement smoothness by assuming that $\log(\mathcal{R}(t))$ is a piecewise polynomial of arbitrary degree. We specifically consider discrete splines with various degrees of continuity. For example, 0th-degree discrete splines are piecewise constant, the 1st-degree curves are piecewise linear, and 2nd-degree curves are piecewise quadratic. For $k \geq 1$, k^{th} -degree discrete splines are continuous and have continuous discrete differences up to degree $k - 1$ at the knots. To achieve such smoothness, we regularize the size of changes between adjacent effective reproduction numbers. Because $\mathcal{R}_t > 0$, we explicitly penalize the divided differences (discrete derivatives) of neighbouring values of $\log(\mathcal{R}_t)$. To achieve this, we penalize the ℓ_1 norm of the divided differences, which introduces sparsity into the curvature, so that the estimates can have heterogeneous smoothness in different periods of time. It is a more realistic setting compared to homogeneous smoothness created by the squared ℓ_2 norm. Using different orders of divided differences result in estimated effective reproduction numbers with different smoothness assumptions.

To enforce smoothness of $\hat{\mathcal{R}}_t$, we add a trend filtering penalty to Eq (4) [23–26]. Let $\theta := \log(\mathcal{R}) \in \mathbb{R}^n$, so that $\Lambda_t = \eta_t \exp(\theta_t)$, and $\log(\eta_t \mathcal{R}_t) = \log(\eta_t) + \theta_t$. For evenly spaced incident case data, we write our estimator as the solution to the optimization problem

$$\hat{\mathcal{R}} = \exp(\hat{\theta}) \quad \text{where} \quad \hat{\theta} = \underset{\theta \in \mathbb{R}^n}{\operatorname{argmin}} \eta^\top \exp(\theta) - \mathbf{y}^\top \theta + \lambda \|D^{(k+1)}\theta\|_1, \quad (4)$$

where $\exp(\cdot)$ applies elementwise. Here, $D^{(k+1)} \in \mathbb{Z}^{(n-k-1) \times n}$ is the $(k+1)^{\text{th}}$ order divided difference matrix for any $k \in \{0, \dots, n-1\}$. $D^{(k+1)}$ is defined recursively as $D^{(k+1)} = D^{(1)}D^{(k)}$, where $D^{(1)} \in \{-1, 0, 1\}^{(n-k-1) \times (n-k)}$ is a sparse matrix with diagonal band:

$$D^{(1)} = \begin{pmatrix} -1 & 1 & & & \\ & -1 & 1 & & \\ & & \ddots & \ddots & \\ & & & -1 & 1 \end{pmatrix}.$$

The tuning parameter λ balances data fidelity with desired smoothness. When $\lambda = 0$, the problem in Eq (4) reduces to the MLE in Eq (3). Larger tuning parameters privilege the regularization term and yield smoother estimates. Finally, there exists λ_{\max} such that any $\lambda \geq \lambda_{\max}$ will result in $D^{(k+1)}\hat{\theta} = 0$ and $\hat{\theta}$ will be the Kullback-Leibler projection of \mathbf{y} onto the null space of $D^{(k+1)}$ (see subsection 2.3).

For unevenly-spaced incidence data, the spacing between neighboring parameters varies with the time between observations, and thus, the divided differences must be adjusted by the times that the observations occur. Given observation times $\mathbf{x} = (x_1, \dots, x_n)^\top$, for $k \geq 1$, define a k^{th} -order diagonal matrix

$$X^{(k)} = \text{diag}\left(\frac{k}{x_{k+1} - x_1}, \frac{k}{x_{k+2} - x_2}, \dots, \frac{k}{x_n - x_{n-k}}\right).$$

Letting $D^{(\mathbf{x},1)} := D^{(1)}$, then for $k \geq 1$, the $(k+1)^{\text{th}}$ -order divided difference matrix for unevenly spaced data can be created recursively by $D^{(\mathbf{x},k+1)} := D^{(1)}X^{(k)}D^{(\mathbf{x},k)}$. No adjustment is required for $k = 0$.

Due to the penalty structure, this estimator is locally adaptive, meaning that it can potentially capture local changes such as the initiation of control measures. [11,12] considered only the 2nd-order divided difference of \mathcal{R}_t rather than its logarithm. In comparison to their work, our estimator (1) allows for arbitrary degrees of temporal smoothness and (2) avoids the potential numerical issues of penalizing/estimating positive real values. Furthermore, as we will describe below, our procedure is computationally efficient for estimation over an entire sequence of penalty strengths λ and provides methods for choosing how smooth the final estimate should be.

2.3 Solving over a sequence of tuning parameters

We can solve the Poisson trend filtering estimator over an arbitrary sequence of λ that produces different levels of smoothness in the estimated curves. We consider a candidate set $\boldsymbol{\lambda} = \{\lambda_m\}_{m=1}^M$, which is a strictly decreasing λ sequence.

Let $D := D^{(k+1)}$ for simplicity in the remainder of this section. As $\lambda \rightarrow \infty$, the penalty term $\lambda\|D\theta\|_1$ dominates the Poisson objective, so that minimizing the objective is asymptotically equivalent to minimizing the penalty term, which results in $\|D\theta\|_1 = 0$. In this case, the divided differences of θ with order $k+1$ is always 0, and thus, θ must

lie in the null space of D , that is, $\theta \in \mathcal{N}(D)$. The same happens for any λ beyond this threshold, so define λ_{\max} to be the smallest λ that produces $\theta \in \mathcal{N}(D)$. It turns out that this value can be written explicitly as $\lambda_{\max} = \|(D^\dagger)^\top (\eta - y)\|_\infty$, where D^\dagger is the (left) generalized inverse of D satisfying $D^\dagger D = I$. Therefore, we use $\lambda_1 = \lambda_{\max}$ and then choose the minimum λ_M to be $r\lambda_{\max}$ for some $r \in (0, 1)$ (typically $r = 10^{-5}$). Given any $M \geq 3$, we generate a sequence of λ values to be equally spaced on the log-scale between λ_1 and λ_M .

2.4 Choosing a final λ

We estimate model accuracy over the candidate set through K -fold cross validation (CV) to choose the best tuning parameter. Specifically, we divide \mathbf{y} (except the first and last observations) roughly evenly and randomly into K folds, estimate \mathcal{R}_t for all $\boldsymbol{\lambda}$ leaving one fold out, and then predict the held-out observations. Model accuracy can be measured by multiple metrics such as mean squared error $\text{MSE}(\hat{y}, y) = n^{-1} \|\hat{y} - y\|_2^2$ or mean absolute error $\text{MAE}(\hat{y}, y) = n^{-1} \|\hat{y} - y\|_1$, but we prefer to use the deviance, to mimic the likelihood in Eq (3): $D(y, \hat{y}) = \frac{1}{n} \sum_{i=1}^n 2(y_i \log(y_i) - y_i \log(\hat{y}_i) - y_i + \hat{y}_i)$, where we define $0 \log(0) = 0$.

To estimate the sequence efficiently, the model is fitted sequentially by visiting each component of $\boldsymbol{\lambda}$ in order. The estimates produced with a larger λ are used as the initial values (warm starts) for the next smaller λ . By solving through the entire sequence of tuning parameters, we have a better chance to achieve a better trade-off between bias and variance, and accordingly, improved accuracy relative to procedures examining one fixed value of λ . Note that for any K and any M , we will end up estimating the model $(K + 1)M$ times rather than once.

2.5 Approximate confidence bands

We also provide empirical confidence bands of the estimators with approximate coverage guarantees. Consider the related estimator $\tilde{\mathcal{R}}_t$ defined as

$$\tilde{\mathcal{R}} = \exp(\tilde{\theta}) \quad \text{where} \quad \tilde{\theta} = \underset{\theta \in \mathbb{R}^n}{\text{argmin}} \quad \eta^\top \exp(\theta) - \mathbf{y}^\top \theta + \lambda \|D\theta\|_2^2.$$

Let $\tilde{\mathbf{y}} = \eta \circ \mathcal{R}$, and then it can be shown (for example, Theorem 2 in [27]) that an estimator for $\text{Var}(\tilde{\mathbf{y}})$ is given by $(\text{diag}(\tilde{\mathbf{y}}^{-2}) + \lambda D^\top D)^\dagger$. Finally, an application of the delta method shows that $\text{Var}(\tilde{\mathbf{y}}_t)/\eta_t^2$ is an estimator for $\text{Var}(\tilde{\mathcal{R}}_t)$ for each $t = 1, \dots, n$. We therefore use $(\text{diag}(\tilde{\mathbf{y}}^{-2}) + \lambda D^\top D)_t^\dagger/\eta_t^2$ as an estimator for $\text{Var}(\hat{\mathcal{R}}_t)$. An approximate $(1 - \alpha)\%$ confidence interval then can be written as $\hat{\mathcal{R}} \pm T(\alpha/2, n - \text{df})s$, where s_t is the square-root of $\text{Var}(\hat{\mathcal{R}}_t)$ for each $t = 1, \dots, n$ and df is the number of changepoints in $\tilde{\theta}$ plus $k + 1$.

2.6 Bayesian perspective

Unlike many other methods for \mathcal{R}_t estimation, our approach is frequentist rather than Bayesian. Nonetheless, it has a corresponding Bayesian interpretation: as a state-space model with Poisson observational noise, autoregressive transition equation of degree $k \geq 0$, e.g., $\theta_{t+1} = 2\theta_t - \theta_{t-1} + \varepsilon_{t+1}$ for $k = 1$, and Laplace transition noise $\varepsilon_{t+1} \sim \text{Laplace}(0, 1/\lambda)$. Compared to **EpiFilter** [8], we share the same observational assumptions, but our approach has a different transition noise. **EpiFilter** estimates the posterior distribution of \mathcal{R}_t , and thus it can provide credible interval estimates as well. Our approach produces the maximum *a posteriori* estimate via an efficient convex optimization, obviating the need for MCMC sampling. But the associated confidence bands are created differently.

3 Results

Implementation of the our approach is provided in the R package **rtestim**. All experiments are run in R with version 4.3.1 on a MacBook with an Apple M1 Pro chip and 32GB RAM running under macOS Sonoma 14.0. The R packages used for simulation and real-data application are versions **EpiEstim** 2.2-4, **EpiLPS** 1.2.0, and **rtestim** 0.0.4.

3.1 Simulation settings

We simulate four scenarios of the time-varying effective reproduction numbers, intended to mimic different epidemics. The first two scenarios are simple cases that are rapidly controlled by intervention, where the graphical curves consist of one discontinuity and

two segments. Scenario 1 has constant \mathcal{R}_t before and after an intervention, while
 Scenario 2 grows exponentially, then decays. The other two scenarios are more
 complicated, where more waves in the epidemics are involved. Scenario 3 has four linear
 segments with three discontinuities, which reflect the effect of an intervention,
 resurgence to rapid transmission, and finally suppression of the epidemic. Scenario 4
 involves sinusoidal waves throughout the epidemic. The first three scenarios and the last
 scenario are motivated by [8] and [9] respectively. We name the four scenarios as (1)
piecewise constant, (2) *piecewise exponential*, (3) *piecewise linear*, and (4) *periodic* lines
 or curves respectively.

In all cases, the times of observation are regular, and epidemics are of length
 $n = 300$. Specifically, in Scenario 1, $\mathcal{R}_t = 2, 0.8$ before and after $t = 70$. In Scenario 2,
 \mathcal{R}_t increases and decreases exponentially with rates 0.015, 0.005 pre and post $t = 50$. In
 Scenario 3, \mathcal{R}_t is piecewise linear with four discontinuous segments following

$$\begin{aligned} \mathcal{R}(t) = & \left(2.5 - \frac{0.5}{59}(t-1)\right) \mathbf{1}_{[1,60]}(t) + \left(0.8 - \frac{0.2}{49}(t-61)\right) \mathbf{1}_{(60,110]}(t) \\ & + \left(1.7 + \frac{0.3}{39}(t-111)\right) \mathbf{1}_{(110,150]}(t) + \left(0.9 - \frac{0.4}{149}(t-151)\right) \mathbf{1}_{(150,300]}(t), \end{aligned}$$

where $\mathbf{1}_A(t) = 1$, if $t \in A$, and $\mathbf{1}_A(t) = 0$ otherwise. In Scenario 4, \mathcal{R}_t is realization of
 the continuous, periodic curve generated by the function

$$\mathcal{R}(t) = 0.2 \left((\sin(\pi t/12) + 1) + (2 \sin(\pi t/6) + 2) + (3 \sin(\pi t/1.2) + 3) \right),$$

evaluated at equally spaced points $t \in [0, 10]$. These settings are illustrated in the left
 column of Fig 2.

We assume that the serial interval follows Gamma distribution with fixed shapes and
 scales (3, 3), (2.5, 2.5), (3.5, 3.5) and (3.5, 3.5) for Scenarios 1–4 respectively. We
 consider all epidemics starting from $y_1 = 2$ cases and generating until timepoints
 $t = 300$. We compute the expected incidence Λ_t using the renewal equation, and
 generate the incidence samples from the Poisson distribution $y_t \sim \text{Pois}(\Lambda_t)$. To verify
 the performance of our model under the violation of this distributional assumption of
 incidence, we also generate incidence samples using the negative Binomial distribution
 with dispersion size 5, i.e., $y_t \sim \text{NB}(\Lambda_t, \text{size} = 5)$. We generate 50 random samples for

each setting of experiments, resulting in 400 total experiments. An example of each effective reproduction number scenario with a single corresponding Poisson and negative Binomial sample incidence sequences is displayed in Fig 2.

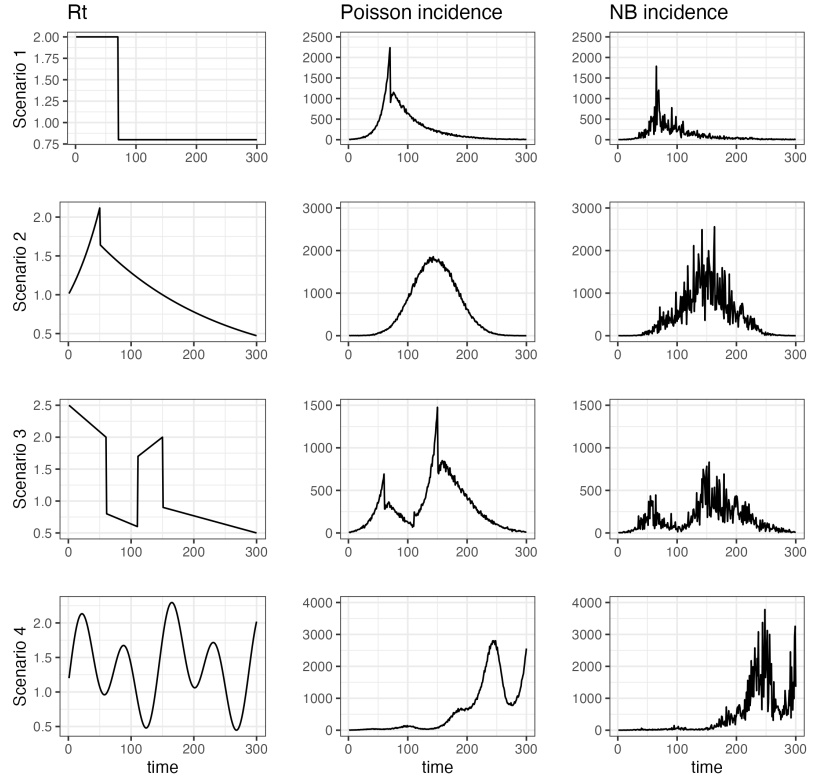


Fig 2. The effective reproduction numbers (left column) and corresponding sample incident cases drawn from a Poisson (middle column) or negative Binomial (right column) distribution. The rows correspond to the four \mathcal{R}_t settings.

We compare `RtEstim` to `EpiEstim` and `EpiLPS`. Unfortunately, `EpiFilter` frequently fails to converge due to the large case counts in many simulations. `EpiEstim` estimates the posterior distribution of effective reproduction numbers given a Gamma prior and Poisson distributed incidence. It estimates the reproduction number over a sliding window, assuming the reproduction number is constant during the specific time window. A longer sliding window averages out more fluctuations, leading to smoother estimates, whereas, a shorter sliding window is more responsive to sudden spikes or declines. We tried the default, a weekly sliding window, as well as a monthly window. However, since neither considerably outperforms the other across all scenarios, we defer the monthly case to the Appendix. `EpiLPS` is another Bayesian approach that estimates P-splines coupled with Laplace approximations of the conditional posterior based on the

negative Binomial likelihood. For **RtEstim** on the four scenarios respectively, we
estimate (1) piecewise constant $k = 0$, (2) piecewise linear & cubic $k = 1, 3$, (3)
piecewise linear $k = 1$ and (4) piecewise cubic polynomials $k = 3$. In each case, we
examine a grid of 50 λ values, selecting the best using 10-fold cross validation. For all
models and problems, we use the serial interval distribution used to create the data.

To measure estimation accuracy, we compare $\widehat{\mathcal{R}}$ to \mathcal{R} using the Kullback-Leibler
(KL) divergence: a standard metric that measures the distance between two probability
distributions. Since \mathcal{R}_t can be regarded as the expectation of Poisson distribution, we
use the KL divergence for Poisson distributions (averaged across all coordinates) to
measure the accuracy of the \mathcal{R}_t estimates

$$D_{KL}(\mathcal{R} \parallel \widehat{\mathcal{R}}) = \sum_{t=1}^n w_t \left(\mathcal{R}_t \log \left(\frac{\mathcal{R}_t}{\widehat{\mathcal{R}}_t} \right) + \widehat{\mathcal{R}}_t - \mathcal{R}_t \right),$$

where $\mathcal{R} = \{\mathcal{R}_t\}_{t=1}^n$ and $w_t = \eta_t / \sum_t \eta_t$ is the rescaled total infectiousness. To fairly
compare across methods, we drop the estimates during the first week because estimates
from **EpiEstim** do not begin until $t = 8$ (using a weekly window). KL divergence is
more appropriate for measuring accuracy because it connects directly to the Poisson
likelihood used to generate the data, whereas standard measures like the mean-squared
error correspond to Gaussian data. This has the effect of increasing the relative cost of
mistakes when Λ_t is small. Other details of the experimental settings are deferred to the
Appendix.

3.2 Simulation results

RtEstim overall outperforms **EpiEstim** and **EpiLPS** in the experimental study. Fig 3
visualizes the KL divergence across the three models. Under both Poisson and negative
Binomial distributions, **RtEstim** is easily the most accurate across Scenarios 1 and 3:
the median of KL divergence is much lower and the boxes frequently fail to overlap
indicating a better performance than the other two methods across all 50 simulations.
The advantage is less for the negative Binomial case compared to the Poisson case, but
still obvious. **RtEstim** and **EpiLPS** have similar performance in Scenarios 2 and 4. For
the Poisson case, **RtEstim** and **EpiLPS** both have very small KL scores, which are very
close to 0. In Scenario 4, **RtEstim** is slightly better for Poisson and **EpiLPS** is better for

negative Binomial, but the boxes largely overlap each other. **EpiLPS** has a slightly lower median and a smaller IQR in Scenario 2 for the negative Binomial case. The two degrees of **RtEstim** used for Scenario 2 perform very close to each other for both distributions, which implies a low risk of model misspecification. We will examine a single realization of each experiment to investigate these global conclusions in more detail.

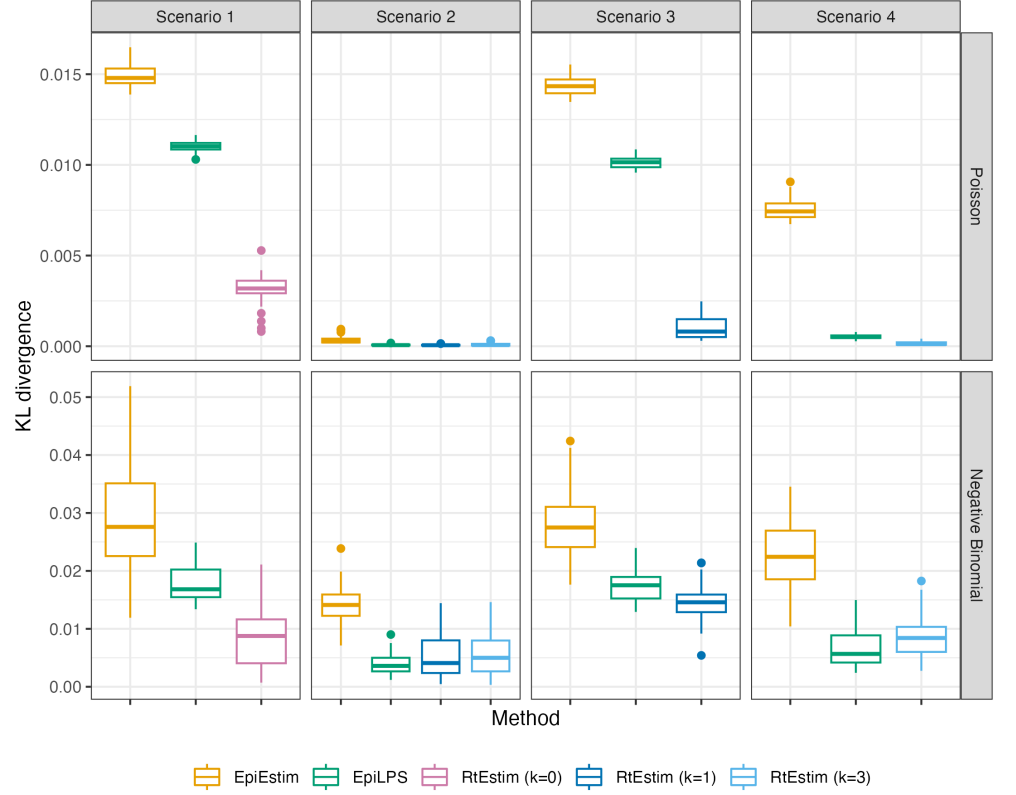


Fig 3. Boxplot of KL divergence between the estimated $\hat{\mathcal{R}}_t$ and the true \mathcal{R}_t across 50 random samples for each approach given Poisson incidence (*in top panels*) and negative Binomial incidence (*in bottom panels*) respectively. Outliers are excluded. Full visualization is deferred to the Appendix.

Fig 4 shows 1 realization for the estimated reproduction numbers under the Poisson generative model for all 4 scenarios. Compared to **EpiEstim** and **EpiLPS**, which have rather severe difficulties at the beginning of the time series, **RtEstim** estimates are more accurate — they nearly overlap with the true values — without suffering from the edge problem. Scenario 2 presents an easy problem in terms of accurate estimation for all methods, except at the change point occurring at the end of the exponential growth. Although the truth is likely best represented with a piecewise cubic curve, the actual curvature is so gentle that linear estimation ($k = 1$) appears potentially reasonable. We,

therefore, fit piecewise linear and cubic $\hat{\mathcal{R}}_t$ curves using **RtEstim** for Scenario 2 to evaluate model misspecification. However, **RtEstim** with both degrees have difficulty recovering the acute rise in the growth phase. Due to this, **RtEstim** has difficulty in convergence and can require more than 10^7 iterates for all models across the λ sequence and 10-fold CV to converge in a couple of simulation samples. An explanation of such failure is that the model imposes discontinuity at the changepoint, which hinders the estimates from fitting the two discontinuous phases. Scenario 1 is the simplest case with only one knot and two constant segments. Besides the edge problem, **EpiEstim** and **EpiLPS** produce “smooth” estimated curves that are continuous at the changepoint, which results in large mistakes in that neighbourhood. Since the piecewise constant **RtEstim** estimator does not force any smoothness in \mathcal{R}_t , it easily captures the sharp change.

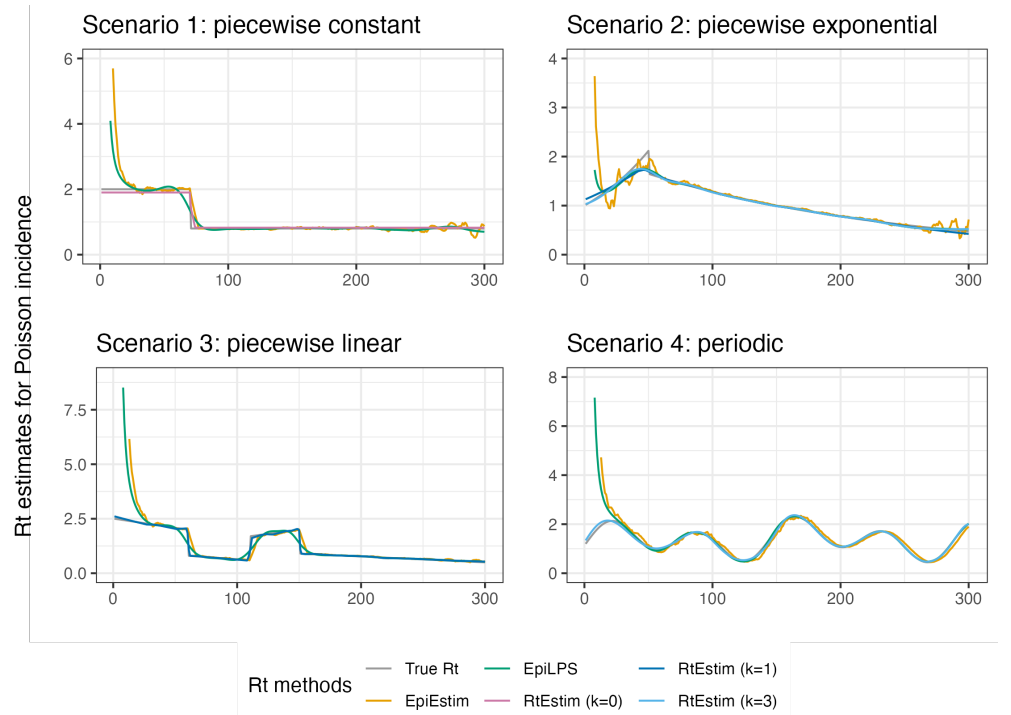


Fig 4. Example of effective reproduction number estimation for Poisson incidence.

To investigate the performance under the violation of the Poisson distributional assumption (of both **RtEstim** and **EpiEstim**), we also examine estimation accuracy with negative Binomial data. Fig 5 displays a realization, analogous to the previous case, for all methods and scenarios. **RtEstim** has more difficulty relative to the Poisson

incidence setting, especially at the beginning of the outbreak. This is most pronounced in Scenario 4, where **RtEstim** is overly smooth, except in the last wave. In Scenario 2, **RtEstim** successfully captures the changepoint, but suffers from the same problem as in the Poisson setting. In Scenario 3, the piecewise linear **RtEstim** recovers the curvature of \mathcal{R}_t well, but is less accurate than in the Poisson incident cases.

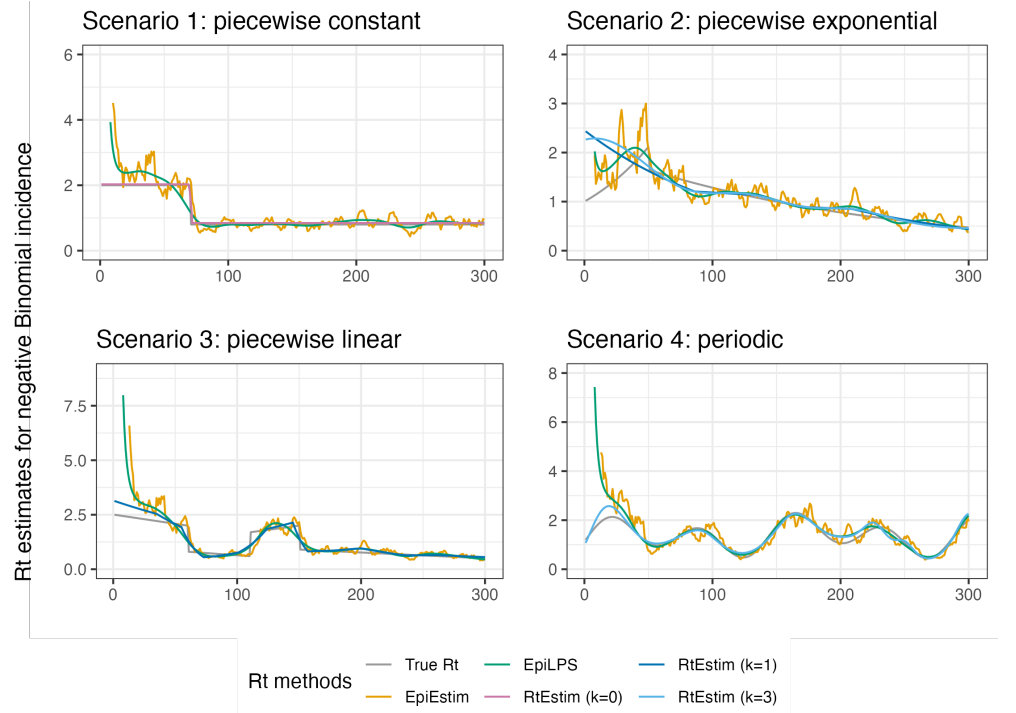


Fig 5. Example of effective reproduction number estimation for negative Binomial incidence.

Finally, it is important to provide a brief comparison of the running times of three models across the 8 experimental settings. We find that almost all models across all experiments complete within 10 seconds. **RtEstim** generally takes the longest, likely due to a relatively large candidate set — 50 values of λ and 10 folds of cross validation — while other models run only a single time for a fixed setting of hyperparameters per experiment. Additional results on timing comparisons are deferred to the Appendix.

3.3 Real-data results: Covid-19 incident cases in British Columbia

We implement `RtEstim` on Covid-19 incident confirmed cases in British Columbia (B.C.) as reported on May 18, 2023 (visualized in Fig 6) by the B.C. Centre for Disease Control. We use the gamma distribution with shape 2.5 and scale 2.5 to approximate the serial interval function, which is empirically reasonable, since they are close to the parameters in a recent study [28], which summarizes estimated parameters of the serial interval distributions of SARS-CoV-2 by different approaches.

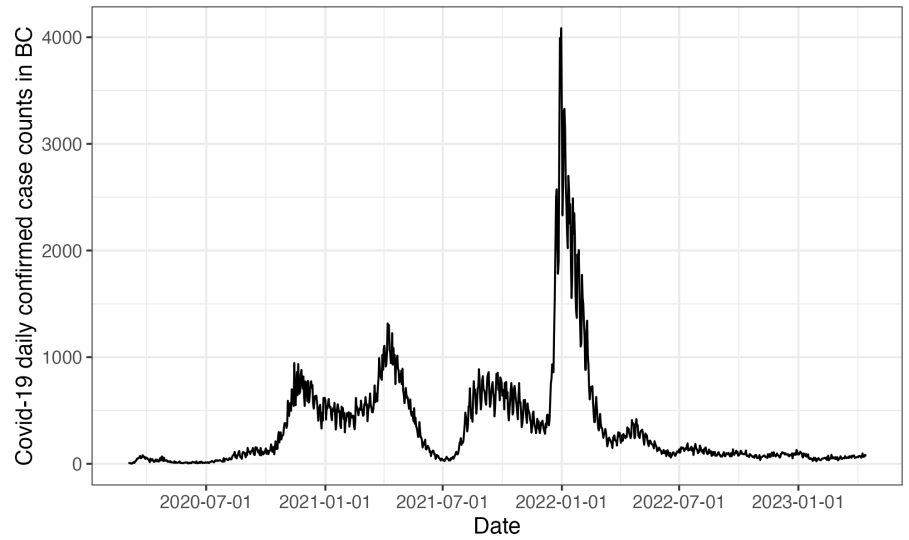


Fig 6. Covid-19 daily confirmed incident cases between March 1st, 2020 and April 15th, 2023 in British Columbia, Canada.

Considering the first, second, and third polynomial degrees, the estimated effective reproduction numbers of Covid-19 in British Columbia (illustrated in Fig 7) are always less than 3 except at the very early stage, which means that one distinct infected individuals on average infects less than three other individuals in the population. Examining three different settings for k , the temporal evolution of $\hat{\mathcal{R}}$ (across all regularization levels λ) are similar near the highest peak around the end of 2021 before dropping shortly thereafter. Throughout the estimated curves, the peaks and troughs of the reproduction numbers precede the growth and decay cycles of confirmed cases, as expected. We also visualize 95% confidence bands for the point estimates at the smallest one of the “optimal” tuning parameters with lowest CV (i.e., KL divergence)

scores in Fig 7.

381

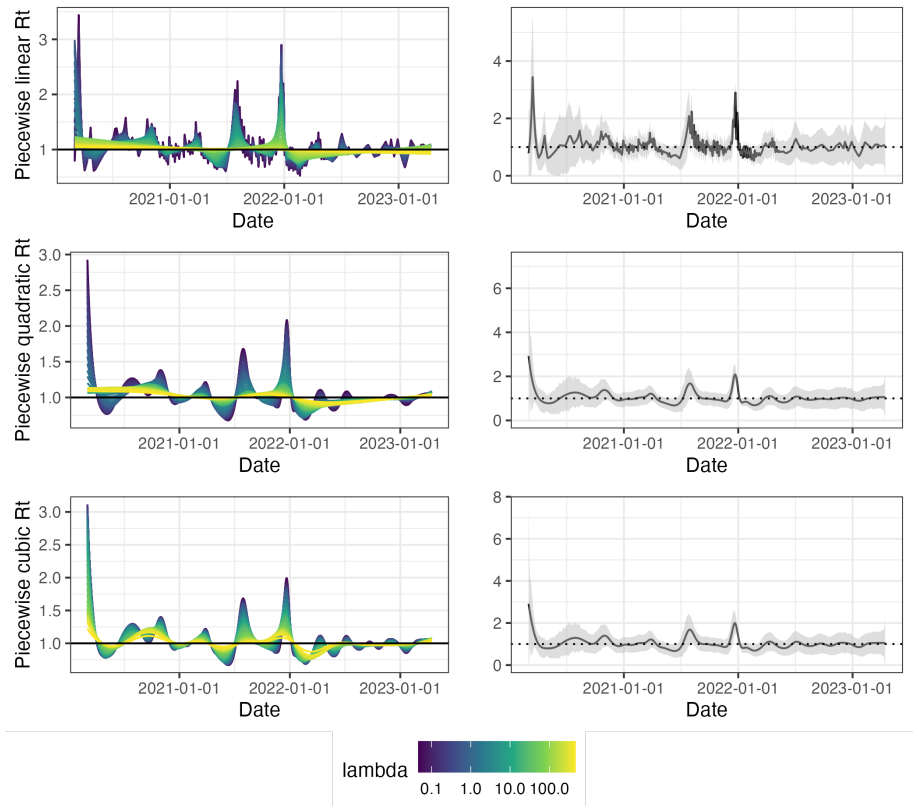


Fig 7. Estimated effective reproduction numbers for Covid19 daily confirmed counts between March 1st, 2020 and April 15th, 2023 in British Columbia, Canada. The left panels demonstrate estimates corresponding to 50 tuning parameters. The right panels display the CV-tuned estimates with 95% confidence intervals. The top, medium and bottom panels illustrate the estimated reproduction numbers (\mathcal{R}_t) using the Poisson trend filtering (in Eq (4)) with degrees $k = 1, 2, 3$ respectively.

The estimated reproduction numbers are relatively unstable before April 1st, 2022. The highest peak coincides with the emergence and global spread of the Omicron variant. The estimated reproduction numbers fall below 1 during two time periods — roughly from April 1st, 2021 to July 1st, 2021 and from January 1st, 2022 to April 1st, 2022. The first trough coincides with the introduction of Covid-19 vaccines in British Columbia. The second trough, shortly after the greatest peak may be due to variety of factors resulting in the depletion of the susceptible population such as increased self-isolation in response to the peak and media and immunity incurred via recent infection. Since around April 1st, 2022, estimated reproduction numbers have remained relatively stable (fluctuating around 1) corresponding to low reported cases (though reporting behaviours have also changed significantly since the Omicron wave).

3.4 Real-data results: Pandemic influenza in Baltimore, Maryland, 1918

We also apply `RtEstim` to daily reported influenza cases in Baltimore, Maryland occurring during the world-wide pandemic of 1918 from September to November. The dataset (shown in Fig 8) is included in the `EpiEstim` R package. The 1918 influenza outbreak, caused by the H1N1 influenza A virus, was unprecedentedly deadly with case fatality rate over 2.5%, infecting almost one-third of the population across the world [29]. The CV-tuned piecewise cubic estimates in Fig 9 better capture the growth at the beginning of the pandemic in Fig 8. The estimated \mathcal{R}_t curve suggests that the transmissibility of the pandemic grew rapidly over the first 30 days before declining below 1 after 50 days. However, it also suggests an increase of the infectiousness toward the end of the period. With the currently available dataset, it is hard to tell if there is a next wave or a steady decline ahead. The CV-tuned piecewise constant and linear estimates in Fig 9 both suggest a steady decline. This is supported by a couple of arguments. The influenza incidence reduces to 0 in the end. The \mathcal{R} estimates of `EpiEstim` with 1-week, 2-week and 4-week sliding windows in [2] are all lower than the threshold 1 in their right tails.

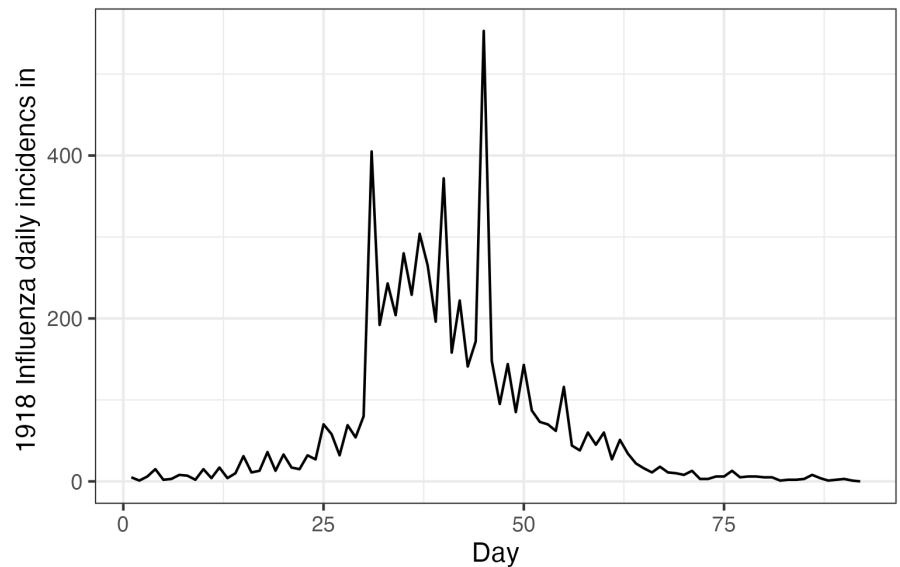


Fig 8. Daily influenza incident counts in Baltimore, Maryland between September and November in 1918.

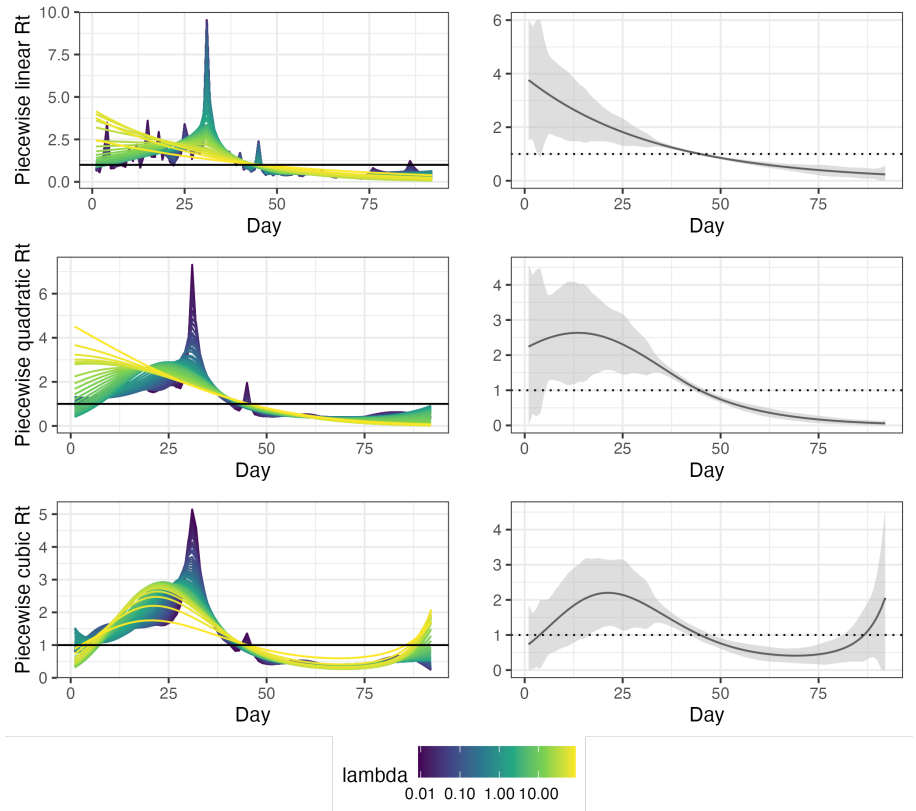


Fig 9. Estimated effective reproduction numbers for influenza in Baltimore, Maryland in 1918. The left panels show estimates for all 50 tuning parameters under consideration. The right column displays the CV-tuned estimates with 95% confidence bands. The rows (top to bottom) show estimated reproduction numbers (\mathcal{R}_t) using the Poisson trend filtering (in Eq (4)) with degrees $k = 1, 2, 3$ respectively.

4 Discussion

The `RtEstim` methodology provides a locally adaptive estimator using Poisson trend filtering on univariate data. It captures the heterogeneous smoothness of effective reproduction numbers given observed incidence data rather than resulting in global smoothness. This is a nonparametric regression model which can be written as a convex optimization (minimization) problem. Minimizing the distance (averaged KL divergence per coordinate) between the estimators and (functions of) observations guarantees data fidelity while the penalty on divided differences between pairs of neighbouring parameters imposes smoothness. The ℓ_1 -regularization results in sparsity of the divided differences, which leads to heterogeneous smoothness within certain periods of time.

The property of local adaptivity (heterogenous smoothness) is useful to automatically distinguish, for example, seasonal outbreaks from outbreaks driven by

other factors (behavioural changes, foreign introduction, etc.). Given a well-chosen polynomial degree, the growth rates can be quickly detected, potentially advising public health to implement policy changes. The effective reproduction numbers can be estimated retrospectively to examine the efficacy of such policies, whether they result in \mathcal{R}_t falling below 1 or the speed of their effects. The smoothness of \mathcal{R}_t curves (including the polynomial degrees and tuning parameters) should be chosen based on the purpose of the study in practice, e.g., epidemic forecasting may require a more wiggly curve that contains more fluctuation information, while retrospective studies that solely target on understanding of the pandemic may prefer a smoother curve with less important information smoothed out.

Our method `RtEstim` provides a natural way to deal with missing data, for example, on weekends and holidays or due to changes in reporting frequency. While solving the convex optimization problem, our method can be easily used to unevenly space or irregularly reported data. Computing the total primary infectiousness is also easily generalized to irregular reporting by modifying the discretization of the serial interval distribution. Additionally, because the ℓ_1 penalty introduces sparsity (operating like a median rather than a mean), this procedure is relatively insensitive to outliers compared to ℓ_2 regularization.

There are a number of limitations that may influence the quality of \mathcal{R}_t estimation. While our model is generic for incidence data, rather than tailored to any specific disease, it does assume that the generation interval is short relative to the period of data collection. More specialized methodologies would be required for diseases with long incubation periods such as HIV or Hepatitis. Our approach, does not explicitly model imported cases, nor distinguish between subpopulations that may have different mixing behaviour. While the Poisson distribution is common, it does not handle overdispersion (observation variance larger than the mean). The negative binomial distribution is a good alternative, but more difficult to estimate in this context. As described in the introduction section, justifying the expression for \mathcal{R} assumes that a relatively constant proportion of true infections is reported. However, if this proportion varies with time (say, due to change in surveillance practices and testing recommendations), the estimates may be biased over this window. A good example is that in early January 2022, during the height of the Omicron wave, British Columbia moved from testing all symptomatic

individuals to testing only those in at-risk groups. The result was a sudden change that would render \mathcal{R}_t estimates on either side of this time point incommensurable.

As currently implemented, `RtEstim` uses a fixed serial interval throughout the period of study, but as factors such as population immunity vary, the serial interval may vary as well [4]. Another issue relates to the equating serial and generation intervals (also mentioned above). The serial interval distribution is generally wider than that of the generation interval, because the serial interval involves the convolution of two distributions, and is unlikely to actually follow a named distribution like Gamma, though it may be reasonably well approximated by one. Our implementation allows for an arbitrary distribution to be used, but requires the user to specify the discretization explicitly, requiring more nuanced knowledge than is typically available. Pushing this analysis further, to accommodate other types of incidence data (hospitalizations or deaths), a modified generation interval distribution would be necessary, and further assumptions would be required as well. Or else, one would first need to deconvolve deaths to infection onset before using our software.

Besides all the advantages and limitations of the methodology discussed above, our `RtEstim` estimator can be implemented easily through a lightweight R package `rtestim` and computed efficiently through the numerical algorithm, proximal Newton method developed in C++, especially for large-scale data. With accessible incident cases, prespecified serial interval distribution, and chosen polynomial degrees, `RtEstim` is able to produce accurate estimation of effective reproduction numbers and provide tuning parameter selection through a path algorithm.

Acknowledgments

xxx

References

1. Cori A, Cauchemez S, Ferguson NM, Fraser C, Dahlgvist E, Demarsh PA, et al.. EpiEstim: estimate time varying reproduction numbers from epidemic curves; 2020.

2. Cori A, Ferguson NM, Fraser C, Cauchemez S. A new framework and software to estimate time-varying reproduction numbers during epidemics. *American Journal of Epidemiology*. 2013;178(9):1505–1512.
3. Thompson RN, Stockwin JE, van Gaalen RD, Polonsky JA, Kamvar ZN, Demarsh PA, et al. Improved inference of time-varying reproduction numbers during infectious disease outbreaks. *Epidemics*. 2019;29:100356.
4. Nash RK, Bhatt S, Cori A, Nouvellet P. Estimating the epidemic reproduction number from temporally aggregated incidence data: A statistical modelling approach and software tool. *PLoS Computational Biology*. 2023;19(8):e1011439.
5. Abbott S, Hellewell J, Thompson RN, Sherratt K, Gibbs HP, Bosse NI, et al. Estimating the time-varying reproduction number of SARS-CoV-2 using national and subnational case counts. *Wellcome Open Research*. 2020;5:112.
6. Abbott S, Funk S, Hickson J, Badr HS, Monticone P, Ellis P, et al.. *epiforecasts/EpiNow2: 1.4.0 release*; 2023.
7. Lison A, Abbott S, Huisman J, Stadler T. Generative Bayesian modeling to nowcast the effective reproduction number from line list data with missing symptom onset dates. *arXiv preprint arXiv:230813262*. 2023;.
8. Parag KV. Improved estimation of time-varying reproduction numbers at low case incidence and between epidemic waves. *PLoS Computational Biology*. 2021;17(9):e1009347.
9. Gressani O, Wallinga J, Althaus CL, Hens N, Faes C. EpiLPS: A fast and flexible Bayesian tool for estimation of the time-varying reproduction number. *PLoS Computational Biology*. 2022;18(10):e1010618.
10. Trevisin C, Bertuzzo E, Pasetto D, Mari L, Miccoli S, Casagrandi R, et al. Spatially explicit effective reproduction numbers from incidence and mobility data. *Proceedings of the National Academy of Sciences*. 2023;120(20):e2219816120.
11. Abry P, Pustelnik N, Roux S, Jensen P, Flandrin P, Gribonval R, et al. Spatial and temporal regularization to estimate COVID-19 reproduction number $R(t)$:

- Promoting piecewise smoothness via convex optimization. PLoS ONE. 2020;15(8):e0237901.
12. Pascal B, Abry P, Pustelnik N, Roux S, Gribonval R, Flandrin P. Nonsmooth convex optimization to estimate the Covid-19 reproduction number space-time evolution with robustness against low quality data. IEEE Transactions on Signal Processing. 2022;70:2859–2868.
 13. Pircalabelu E. A spline-based time-varying reproduction number for modelling epidemiological outbreaks. Journal of the Royal Statistical Society Series C: Applied Statistics. 2023;72(3):688–702.
 14. Ho F, Parag KV, Adam DC, Lau EH, Cowling BJ, Tsang TK. Accounting for the Potential of Overdispersion in Estimation of the Time-varying Reproduction Number. Epidemiology. 2023;34(2):201–205.
 15. Azmon A, Faes C, Hens N. On the estimation of the reproduction number based on misreported epidemic data. Statistics in Medicine. 2014;33(7):1176–1192.
 16. Gressani O, Faes C, Hens N. An approximate Bayesian approach for estimation of the instantaneous reproduction number under misreported epidemic data. Biometrical Journal. 2022;65(6):2200024.
 17. Jin S, Dickens BL, Lim JT, Cook AR. EpiMix: A novel method to estimate effective reproduction number. Infectious Disease Modelling. 2023;8(3):704–716.
 18. Hettinger G, Rubin D, Huang J. Estimating the instantaneous reproduction number with imperfect data: a method to account for case-reporting variation and serial interval uncertainty. arXiv preprint arXiv:230212078. 2023;.
 19. Gostic KM, McGough L, Baskerville EB, Abbott S, Joshi K, Tedijanto C, et al. Practical considerations for measuring the effective reproductive number, R_t . PLoS Computational Biology. 2020;16(12):e1008409.
 20. Pitzer VE, Chitwood M, Havumaki J, Menzies NA, Perniciaro S, Warren JL, et al. The impact of changes in diagnostic testing practices on estimates of COVID-19 transmission in the United States. American Journal of Epidemiology. 2021;190(9):1908–1917.

21. Hitchings MD, Dean NE, García-Carreras B, Hladish TJ, Huang AT, Yang B, et al. The usefulness of the test-positive proportion of severe acute respiratory syndrome coronavirus 2 as a surveillance tool. *American Journal of Epidemiology*. 2021;190(7):1396–1405.
22. Pellis L, Scarabel F, Stage HB, Overton CE, Chappell LH, Fearon E, et al. Challenges in control of COVID-19: short doubling time and long delay to effect of interventions. *Philosophical Transactions of the Royal Society B*. 2021;376(1829):20200264.
23. Kim SJ, Koh K, Boyd S, Gorinevsky D. ℓ_1 trend filtering. *SIAM Review*. 2009;51(2):339–360.
24. Tibshirani RJ. Adaptive piecewise polynomial estimation via trend filtering. *The Annals of Statistics*. 2014;42(1):285–323.
25. Tibshirani RJ. Divided differences, falling factorials, and discrete splines: Another look at trend filtering and related problems. *Foundations and Trends® in Machine Learning*. 2022;15(6):694–846.
26. Sadhanala V, Bassett R, Sharpnack J, McDonald DJ. Exponential Family Trend Filtering on Lattices. *arXiv preprint arXiv:220909175*. 2022;.
27. Vaiter S, Deledalle C, Fadili J, Peyré G, Dossal C. The degrees of freedom of partly smooth regularizers. *Annals of the Institute of Statistical Mathematics*. 2017;69:791–832.
28. Lehtinen S, Ashcroft P, Bonhoeffer S. On the relationship between serial interval, infectiousness profile and generation time. *Journal of the Royal Society Interface*. 2021;18(174):20200756.
29. Taubenberger JK, Morens DM. 1918 Influenza: the mother of all pandemics. *Emerging Infectious Diseases*. 2006;17(1):69–79.

Supplementary details on experiments of effective reproduction number estimation with trend filtering

Jiaping Liu, Zhenglun Cai, Paul Gustafson, and Daniel J. McDonald

2023-12-06

1 Supplementary details on experimental settings of RtEstim for Section 3.1

We run 10-fold cross validation (CV) to choose the best tuning parameter from the candidate set of size 50, i.e., $\lambda = \{\lambda_1, \dots, \lambda_{50}\}$. Specifically, we divide the all samples (except the first and last entries) into ten folds evenly and randomly, and build models on each sample set by leaving a fold out across all hyperparameters. We select the tuning parameter that gives the lowest averaged *deviance* between the estimated reproduction numbers and the observed samples averaged over all folds.

2 Supplementary results of experiments for Fig 3 in Section 3.2

The full KL divergence values for Poisson incidence without excluding the outliers are shown in Fig 10. Y-axis is displayed on a logarithmic scale for a better visualization, since a few values are much larger than others.

Comparing among Rt estimations by EpiLPS, RtEstim and EpiEstim with *weekly* sliding windows, KL values computation excludes the first week of Rt estimates for all approaches. The outliers are mainly EpiLPS and EpiEstim Rt estimations in Scenario 2, which is generally an easy problem except for the changepoint at where the two segments are discontinuous. Since EpiEstim produces a continuous Rt curve, the changepoint can be difficult to recover and make estimation less accurate.

3 Experimental results of methods using monthly sliding windows for Section 3.1

Fig 11 displays the KL divergence values for negative Binomial incidence including the outliers. Comparing across Rt estimations by EpiLPS, RtEstim and EpiEstim with *monthly* sliding windows, KL divergence values computation excludes the first month of Rt estimates for all approaches.

The relative performance of EpiEstim with monthly sliding windows, in general, is not as good as its weekly sliding window based on the relative positions of its boxes and the counterparts of the other methods, except for the Scenario 2 with negative Binomial incidence. A reason is that EpiEstim with longer sliding windows

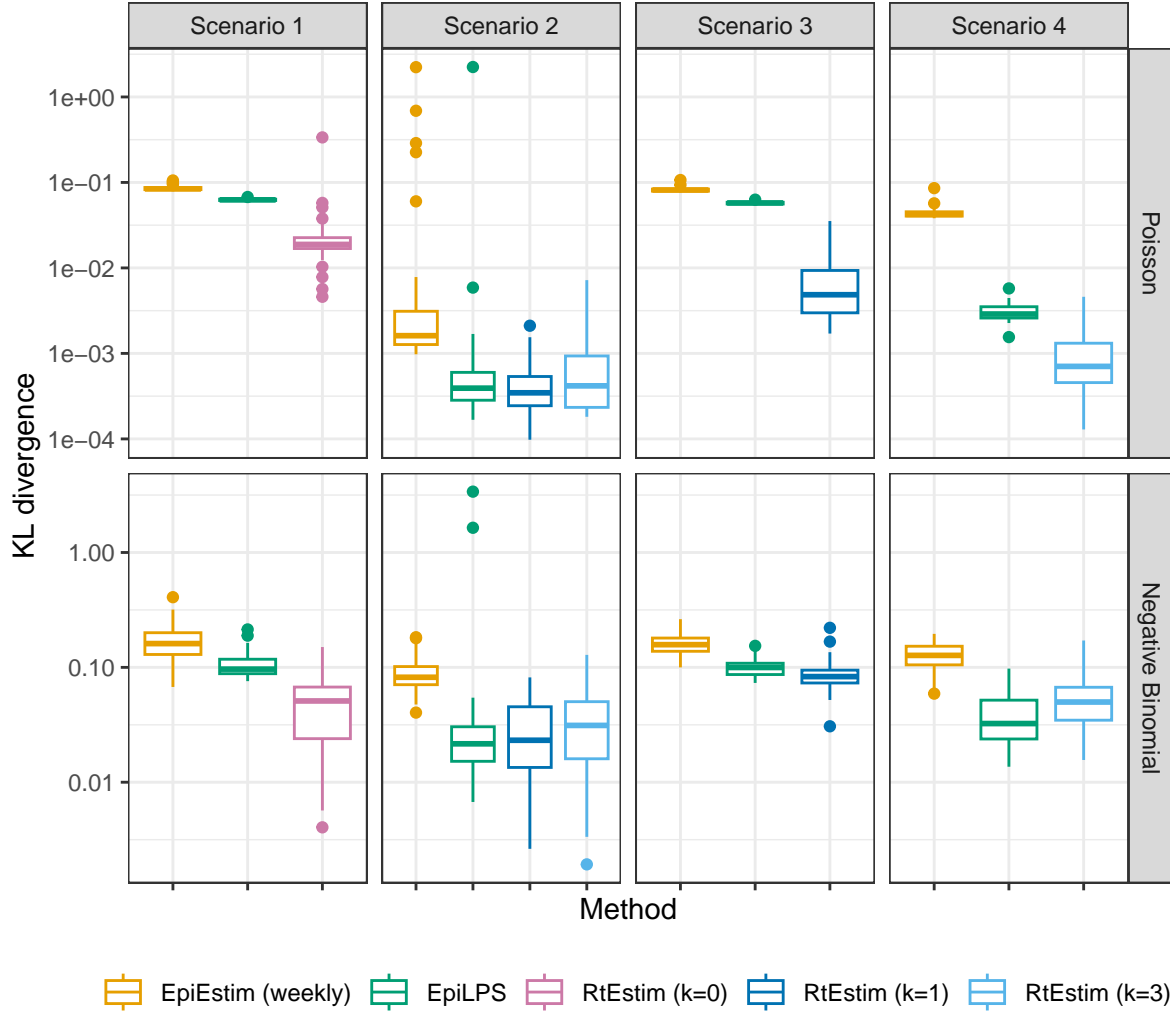


Fig 10. KL divergence for methods with weekly sliding windows. Y-axis is on a logarithmic scale.

assume similarity of neighboring R_t across longer periods, and thus, is smoother and less accurate compared to the one with shorter sliding windows.

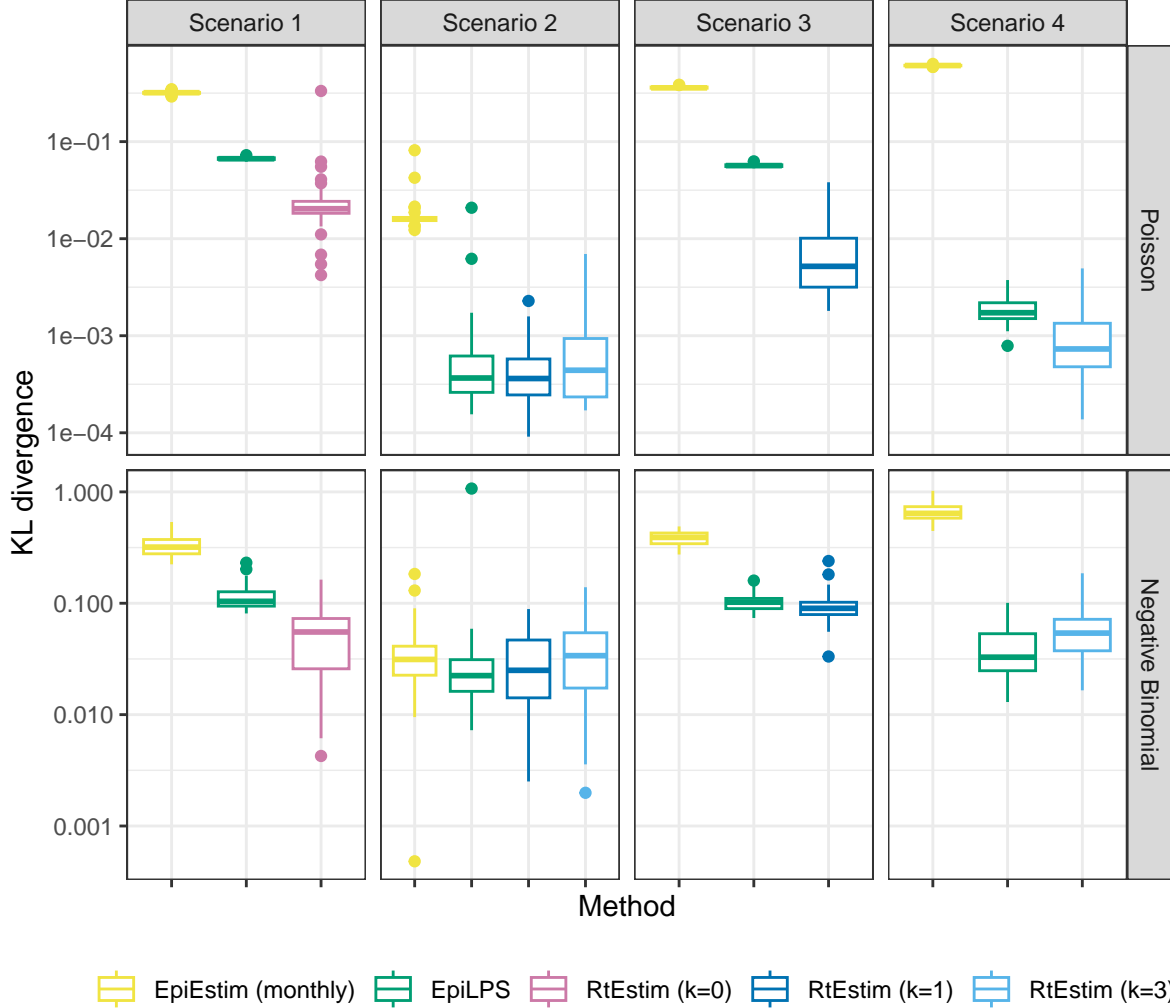


Fig 11. KL divergence for methods with monthly sliding windows. Y-axis is on a logarithmic scale.

4 Time comparisons of methods for Section 3.2

Fig 12 shows the time comparisons across all methods. EpiEstim with both weekly and monthly sliding windows are very fast and converge in less than 0.1 seconds. Piecewise constant RtEstim (with $k=0$) estimates can be generated within 0.1 seconds as well. EpiLPS is slightly slower, but still very fast and within 1 second for all experiments. Piecewise linear and cubic RtEstim (with $k=1$ and 3 respectively) are slower, but mostly within 10 seconds.

It is remarkable that our RtEstim computes 50 lambda values with 10-fold CV for each experiment, which results in 500 times of modelling per experiment. The running times are no more than 10 seconds for most of the experiments, which means the running time for each time of modelling is very fast, and on average can be less than 0.02 seconds. The other two methods only run once for a fixed set of hyperparameters for each experiment.

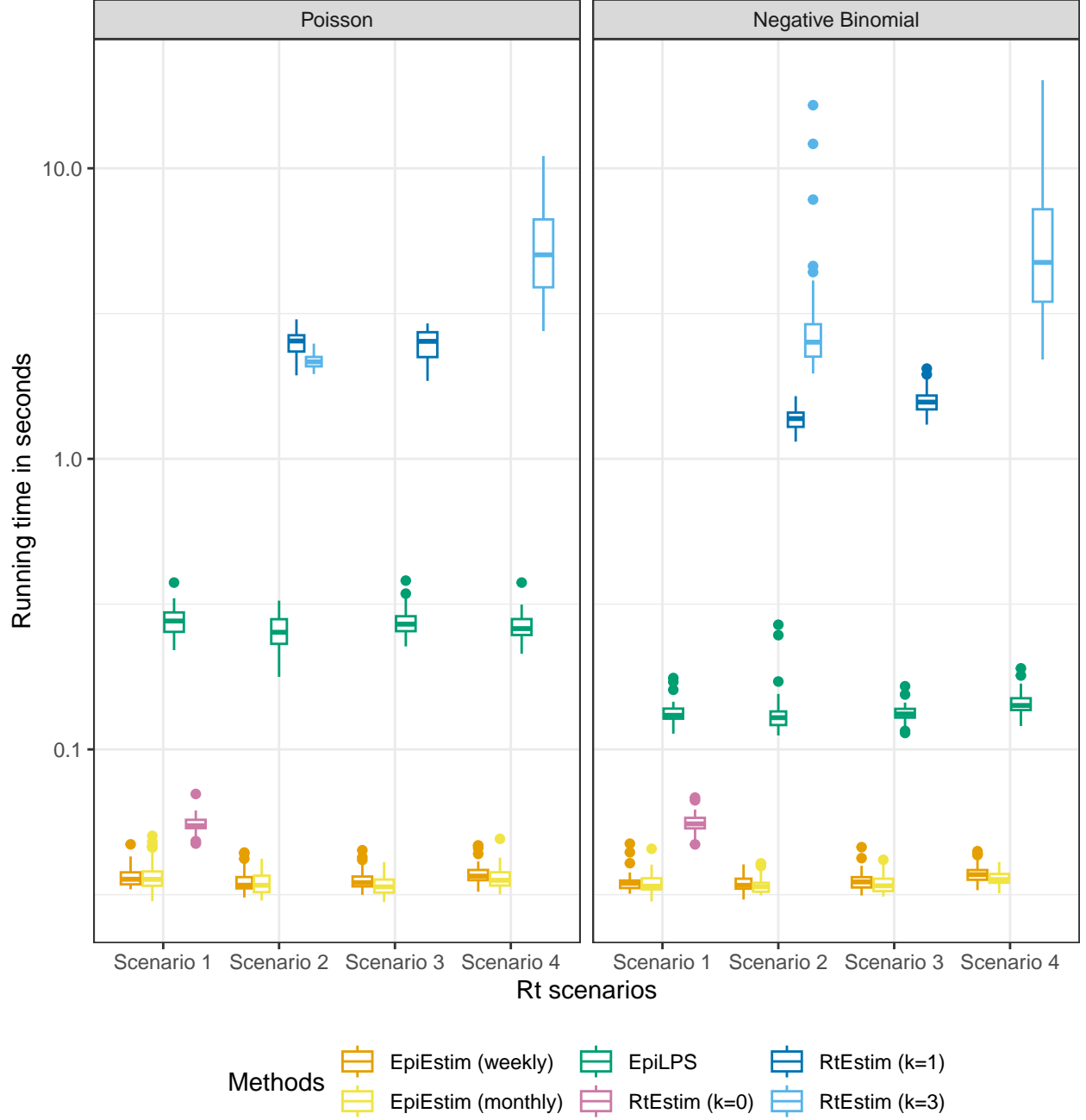


Fig 12. Time comparisons of methods (excluding one outlier of *RtEstim* ($k=1$) in Scenario 2 with negative Binomial incidence). Y-axis is on a logarithmic scale.